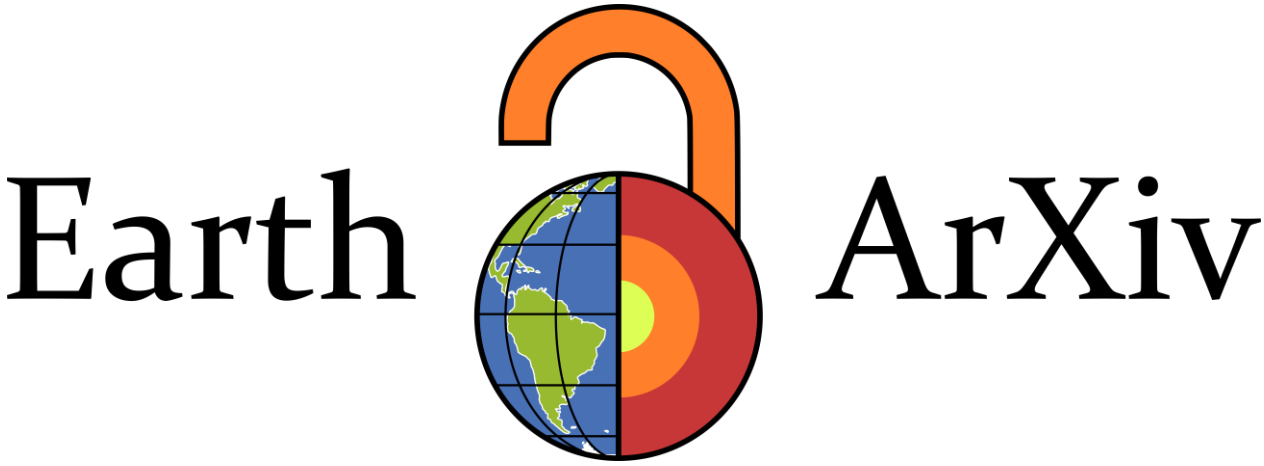

This is a non-peer-reviewed preprint submitted to EarthArXiv.

This manuscript has been submitted for publication in *Science*. Please note the manuscript has yet to be formally accepted for publication. Subsequent versions of this manuscript may have slightly different content. If accepted, the final version of this manuscript will be available via the 'Peer-reviewed Publication DOI' link on the right-hand side of this webpage. Please feel free to contact any of the authors; we welcome feedback.

Title: Reduced geomagnetic shielding increased UV-B radiation at Earth's surface during the *Laschamps Event*

Authors: Timothy J Heaton[1]*, Eloise Wilkinson-Rowe[1,2], Linn Cecilie Krüger[3], Edouard Bard[4], Christine S Lane[5], Amy McGuire[6], T. Matthew Robson[7,8], Takeshi Nakagawa[9], Alistair WR Seddon[10]*

Affiliations:

[1]Department of Statistics, School of Mathematics, University of Leeds; Leeds, LS2 9JT, UK.
*Corresponding author. Email: t.heaton@leeds.ac.uk

[2]School of Archaeology, University of Oxford; Oxford, OX1 3TG, UK.

[3]Department of Biological Sciences, University of Bergen; Bergen, NO-5020, Norway.

[4]CEREGE, Aix-Marseille University, CNRS, IRD, INRAE, Collège de France; Technopole de l'Arbois BP 80, 13545 Aix en Provence Cedex 4, France.

[5]Department of Geography, University of Cambridge; Cambridge, CB2 3EN, UK.

[6]School of Earth and Environment, University of Leeds; Leeds, LS2 9JT, UK.

[7] National School of Forestry, Institute of Science & Environment, University of Cumbria, Rydal Road, Ambleside, Cumbria, LA22 9BB, UK.

[8]Viilkki Plant Science Centre, OEB, Faculty of Biological & Environmental Sciences, University of Helsinki, 00014, Finland

[9]Research Centre for Paleoclimatology, Ritsumeikan University; Shiga, 525-8577, Japan.

[10]Department of Biological Sciences and Bjerknes Center for Climate Research, University of Bergen; Bergen, NO-5020, Norway.
*Corresponding author. Email: alistair.seddon@uib.no

Abstract: Exposure to excess UV-B radiation can harm organisms through DNA damage and oxidative stress, and has likely been a key ecological and evolutionary driver throughout Earth's history. Here, we show UV-B at Earth's surface was significantly increased during the *Laschamps Event,* the last major geomagnetic excursion ca. 41ka BP. During the *Laschamps*, we find significant and prolonged (lasting >600yrs) increases in UV-B absorbing compounds in subfossil *Pinus Diploxylon* pollen (e.g., 31% [95% CI 19-44] increase compared to 1.3ka BP). Furthermore, we identify a significant (negative) broader linear relationship (p<0.001) between UV-B absorbing compounds and the geomagnetic dipole moment extending over the past 65ka. Our results demonstrate an empirical link between surface UV-B and geodynamo strength, important for understanding our past and mitigating our potential future.

Main Text:

The amount of solar UV-B (ultraviolet-B, 280–315nm) radiation reaching Earth's surface has varied considerably over time. Past variations in UV-B radiation have been implicated as a key driver of the ecology and evolution of life on Earth, particularly during mass extinction events at the Permian-Triassic and Devonian-Carboniferous boundaries (*1–5*). The Earth's surface is protected from UV-B radiation by stratospheric ozone. When ozone levels are high, more of the Sun's radiation is attenuated leading to a reduction in the amount of UV-B radiation reaching Earth's surface. The thickness of the stratospheric ozone layer can be substantially influenced by geomagnetic field strength, perturbations to atmospheric composition, and solar activity (*6*).

To date, empirical investigations into past ozone depletion, and consequently increased surface UV-B radiation, have focused on the effects of volcanic eruptions such as the Siberian Traps during the end-Permian (*3*, *4*) and excess chlorine monoxide (ClO) production due to global warming at the end-Devonian (*5*). However, a further potential risk to the ozone layer is a weakening of the geomagnetic field which shields Earth from incoming solar and galactic cosmic rays. Without geomagnetic shielding, it has been hypothesized that the increased penetration of these ionizing, high-energy, particles into Earths' atmosphere would lead to raised NO_x concentrations in the stratosphere and mesosphere, causing the ozone layer to become substantially depleted. This would, in turn, lead to substantially increased UV-B radiation at Earth's surface (*7–10*).

This mechanism has been linked to potential ecological and climatic change during the most recent major geomagnetic excursion, the *Laschamps Event*, which occurred from 42–40ka BP (*11*, *12*). Indeed, excess UV-B radiation at this time has been proposed as a major factor in *Neanderthal* extinction (*7*, *9*, *10*, *13*). Recent modelling of atmospheric chemistry has proposed that, during the *Laschamps* excursion, surface UV-B radiation would have increased by 5% in active sun periods and by up to 10–15% during Grand Solar Minima, compared to the present-day (*9*); while it has been suggested a coincident extreme solar particle event could have led to a short-term, 6yr, increase of 20–30% (*8*). This hypothesis, of increased surface UV-B during the *Laschamps Event*, and the impacts on ecology and the *Neanderthals*, is however highly contested (*14*, *15*).

Understanding the potential impacts of a weakened geodynamo is particularly important as the intensity of the geomagnetic field has been continuously decaying, at a rate of 5% per century, since the first instrumental measurements were made in AD1840 (*16*, *17*). This has led to speculation we are entering a period of substantial weakening and potentially another excursion/reversal. Forecasting the future effects of this ongoing geodynamo decrease is vital to identify potential dangers (*16*, *18*). Support for the hypothesized impacts of geomagnetic field variations and reversals on UV-B radiation is however currently reliant upon circumstantial evidence due to coincident timing and/or model-based estimates (*7–10*, *19–23*). Direct observational evidence is speculative and limited, invoking tentative linkages between the *Laschamps Event*, atmospheric ozone, and sulfur isotope anomalies in non-volcanic sulfate extracted from Antarctic ice (*24*).

Scope:

Objectives

We aim to test two fundamental questions/hypotheses, which we address through a structured experimental design to increase inferential power. Firstly, we investigate whether there is evidence for a relationship between surface UV-B irradiance and geomagnetic field strength as measured by the axial dipole moment (ADM). Specifically, whether a reduction in dipole power is

accompanied by an increase in surface UV-B. Secondly, we test whether there is evidence of significantly increased UV-B irradiance during the *Laschamps Event* (ca. 41ka BP). These hypotheses are tested using a biomolecular approach that quantifies the amount of UV-B absorbing compounds found in the sporopollenin of subfossil pollen grains (*25–32*). We use *Pinus Diploxylon (Pinus D.)* pollen grains obtained from the annually laminated Japanese Lake Suigetsu sediment record (*33*, *34*).

Experimental Design

We targeted five time periods over the last 70ka for analysis, centered on: 1.3, 8, 41, 53 and 65ka BP (Fig. 1A). These periods were selected to cover a combination of both geomagnetic field strengths and pollen calendar ages with low collinearity. Each selected period was further split into four contiguous 150yr sampling intervals. This resulted in twenty sampling intervals, split into five distinct experimental blocks (Fig. 1B–F). Our primary outcome was replicated at least three times in each interval (see Measured Outcomes).

Such a design allows us to distinguish between pollen effects due to geomagnetic variations and those due to potential grain degradation over time, a possible nuisance variable. Our replication within and across independent, but adjacent, 150yr intervals further increases inferential robustness.

Our design included the geomagnetic dipole moment extremes over the past 70ka: the highest dipole moments occurring around 1ka and 53ka BP when the geodynamo was at its strongest; and the lowest dipole moment levels seen during two global geomagnetic excursions, the *Laschamps Event* at 41ka BP, and the (less substantial) *Norwegian-Greenland Sea* excursion around 65ka BP (*35*, *36*). Periods known to contain high sulfur and/or halogen-emitting volcanic eruptions were excluded from consideration to reduce the likelihood any observed variations in UV-B were a consequence of volcanic, rather than paleomagnetic, factors.

The SG06 sediment core from Lake Suigetsu, Japan (SG06; 35°35′0″N, 135°53′0″E) spans the last 150ka. Due to the preservation of annual laminations extending back ~70ka, and supported by extensive radiocarbon and tephra dating, the lake has a highly precise age model covering our study period which facilitates our detailed sampling (*33*, *37*, *38*).

We selected the expected (global) ADM, specifically the GGF100k reconstruction, for each 150yr interval as our primary explanatory variable (*35*, *36*). While a localized paleomagnetic estimate from Lake Suigetsu sediment (*39*) is available, the increased likelihood of substantial non-dipole moments during the *Laschamps Event* (*40*) mean that the global GGF100k compilation provides a more reliable measure of the shielding provided by the geomagnetic field. Potential differences between the GGF100k and Lake Suigetsu chronologies were considered when calculating the expected ADM value for a particular sediment sample. See Materials and Methods for details.

Measured Outcomes

Our primary measured outcome is the amount of UV-B absorbing *para*-Coumaric acid (*p*-CA) within the *Pinus D.* grains of each 150yr sampled interval. This was quantified using pyrolysis-Gas Chromatography Mass Spectrometry (py-GC-MS). For each of our twenty sampled 150yr intervals, a minimum of three independent replicates were analysed. In those sections where more pollen was available, the number of replicates was increased to five or six. In total, 72 replicates were measured. We aimed for each replicate to contain 100 grains (three replicates had fewer due to lower pollen concentrations).

We also considered, as a secondary outcome, the *Pinus D.* grain malformation rate. Higher pollen malformation rates are known to indicate increased environmental stress during sporogenesis (*1*, *41–44*) and therefore reflect environmentally-induced mutagenesis (*45*). Laboratory experiments have demonstrated the malformation response to various UV-B irradiation treatments, although extremely high irradiances are required to induce such changes (*1*). For each 150yr interval, a random sample of grains was isolated, and counts made of both the number of phenotypically normal (i.e., central corpus and two sacci) and malformed grains. Malformed grains (Fig. S5) were defined as those having either fewer, or more, than two sacci, as well as conjoined or fused grains (*46*). Where more material was available, two replicates were obtained from independent sediment preparations. In total 39 samples were prepared for counting, with eight over the *Laschamps Event* (two replicates for each 150yr section).

All statistical analysis (see Materials and Methods) was performed at the individual replicate level to increase robustness of inference.

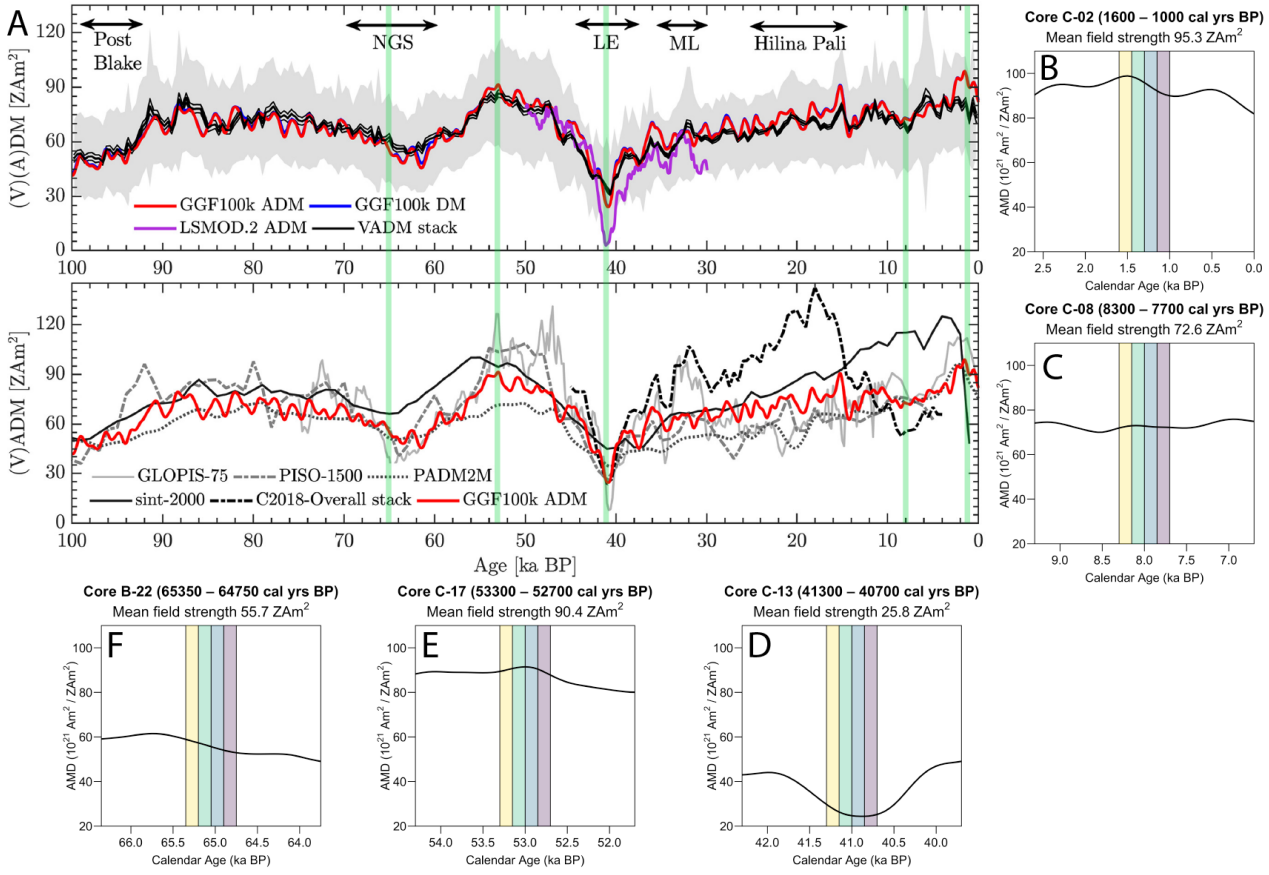

Figure 1 Experimental Design of Sampling. Panel A, modified from (36): Various (virtual) axial dipole moment (V)ADM reconstructions of geomagnetic field strength over the last 100ka are plotted as continuous lines. We use the GGF100k ADM reconstruction (red curve with grey area showing its 1σ interval) as our explanatory variable. Also shown are the five time periods centered on 1.3, 8, 41, 53 and 65ka BP (vertical green shaded boxes). Panels B-E show in detail, for each of these periods, the GGF100k ADM reconstruction. In each period, the four disjoint 150yr intervals from which we sample subfossil pollen are shown as variously colored shaded intervals. The mean expected ADM over each broader (600yr) period is stated in the individual panel titles,

although when fitting our linear model to the amounts of p-CA measured in each sample, the specific value for the 150yr interval is used. Panel A is annotated with proposed geomagnetic excursions (black text) with double-headed arrows indicating their timings (NGS: Norwegian-Greenland Sea, LE: Laschamps, and ML: Mono Lake excursion). See (36) for further explanation.

5

Results

Relationship between p-CA and geomagnetic field strength

The p-CA levels in our 72 replicates are shown in Fig. 2. A linear model fitted to the individual replicates that includes the ADM, as well as the calendar age of the subfossil grains to account for potential biomolecular degradation over time, shows strong evidence (*p-value* < 0.001) for a negative relationship between the geomagnetic ADM and *p*-CA levels in the sporopollenin (Fig. 2A). A decrease in geomagnetic field strength of 1 ZAm^2 is estimated to lead to an expected increase in *p*-CA of 1.73×10^{-3} ng $grain^{-1}$ (95% CI of $[1.16, 2.31] \times 10^{-3}$ ng $grain^{-1}$). There is no evidence for an effect of the calendar age of the subfossil grains (*p-value* = 0.63) on *p*-CA levels. Model checking (diagnostics, Fig. S4) suggests these two explanatory variables, the ADM at the time of grain formation and the grain age, provide a satisfactory fit to the measured *p*-CA content in the individual replicates. Together, the linear model explains 40% (R^2) of the variance in the measured *p*-CA content across the replicates (F-statistic = 22.6 with 2 and 69 degrees of freedom, *p-value* < 0.001).

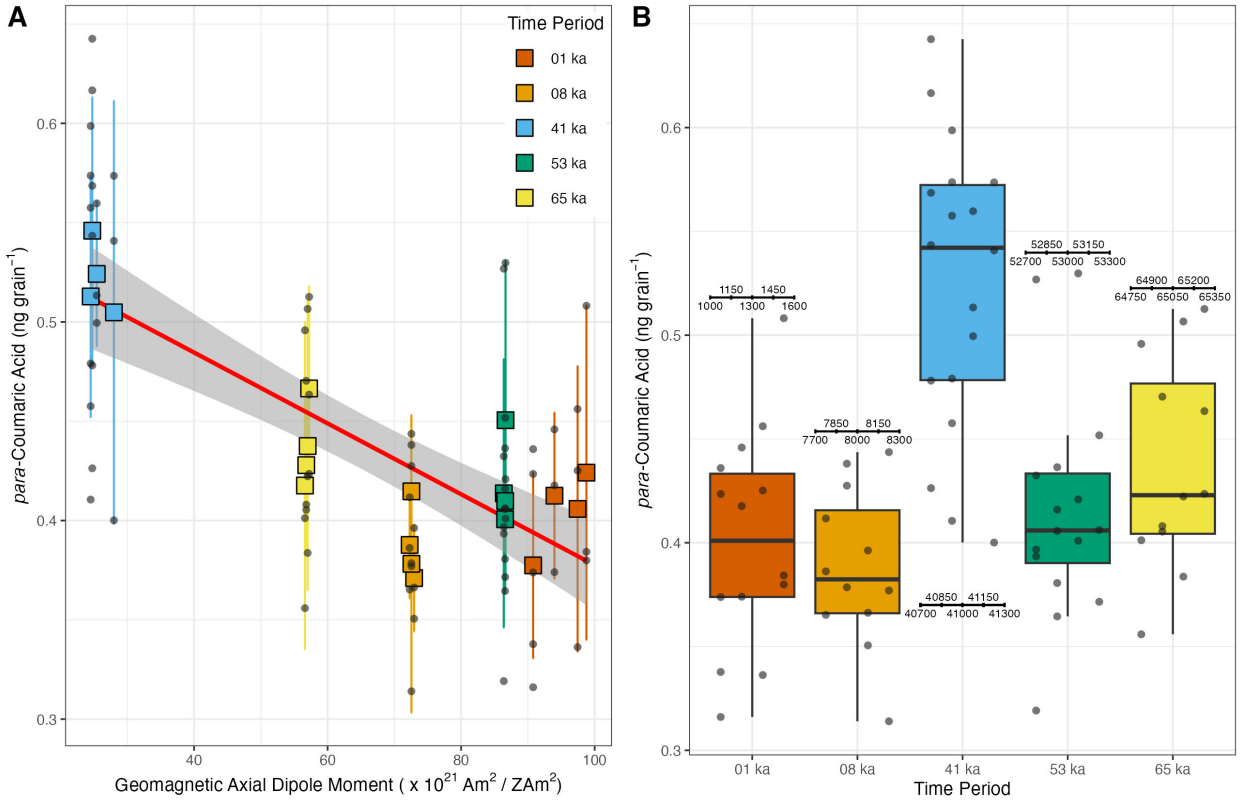

Figure 2 Biochemical changes in each sampled section of Lake Suigetsu sediment (20 sections in total, each spanning an independent 150yr interval, covering five broader 600yr time periods centred around 1.3, 8, 41, 53 and 65ka BP). Panel A: Measured p-CA content in all 72 replicates compared to expected geomagnetic ADM at corresponding time (grey dots). An indication of the linear relationship between the two is shown by the solid red line (with its 95% confidence shaded interval). The sample p-CA mean (and associated 95% intervals) for each of our 20 independently sampled 150yr sections are shown as solid squares. Panel B: Boxplots of p-CA content in each broad 600yr period. Solid dots show the p-CA content measured in all individual replicates,

plotted according to the individual 150yr interval from which they were sampled (see accompanying calendar sub-scale).

Geochemical Evidence for Enhanced Surface UV-B Radiation During the Laschamps Event

The increases in *p*-CA during the *Laschamps Event* are persistent, present over a prolonged period of at least 600 years lasting from 41.3–40.7ka BP. The mean *p*-CA contents recorded in all four disjoint 150yr sections sampled over this period are uniformly higher than in all the other 16 sections sampled (Fig. 2A, blue solid squares lie above all squares in other sections).

During the *Laschamps Event*, the mean amount of UV-B absorbing *p*-CA within each *Pinus D.* grain is estimated to have increased by 31% (with a 95% CI of [19, 44]%) compared to those grains from 1.3ka BP; by 35% ([22, 51]%) compared to 8ka BP; 26% ([15, 38]%) compared to 53ka BP; and 20% ([9, 32]%) compared to 65ka BP.

Given the expected relationship between the accumulation of UV-B absorbing compounds in plants and UV-B surface irradiance (*47*), the recorded *p*-CA increase provides extremely strong evidence for a substantial increase in surface UV-B radiation during the *Laschamps Event*.

Non-significant changes in Pinus D. malformation rate

Fig. 3 shows the grain malformation rates for our 39 sampled replicates. The observed proportions display overdispersion. This is expected since the numbers of malformed grains are small (typically < 1%) and, due to the sampling process, there is likely to be some dependence between the grains isolated. If malformations are not uniformly distributed throughout the entire 150yr sampling interval, particularly if there are short sub-intervals with higher malformation rates, individual replicates may over/under sample malformed grains. We account for this extra variation using a binomial logistic regression, using the broad time period as our explanatory variable, that is adapted to incorporate over-dispersion and fitted using quasi-likelihood (*48*).

While we see some suggestion of a small increase in the probability of malformation during the *Laschamps* compared to the other time periods, the evidence for this is weak (*p-value* = 0.12, 0.37, 0.04, and 0.16 when compared to the malformation probabilities in the 1.3, 8, 53 and 65ka BP periods respectively).

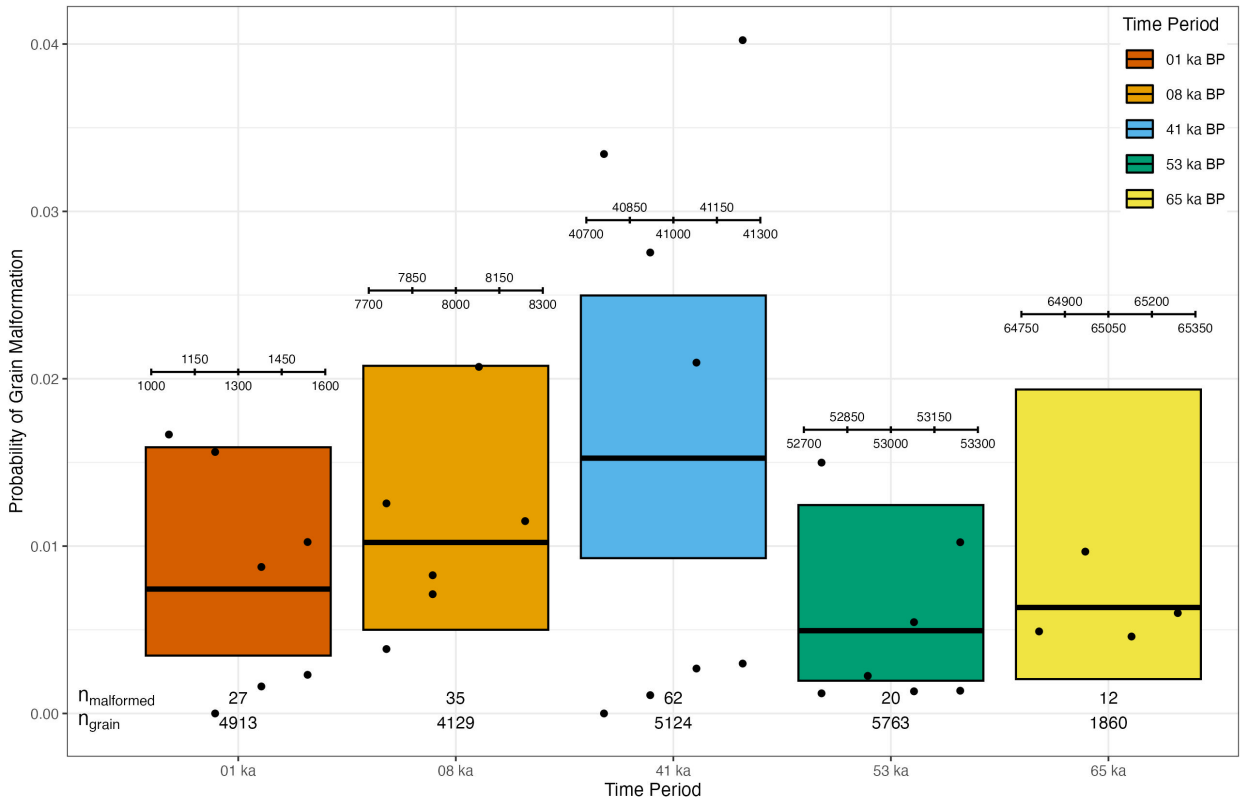

Figure 3 Comparison of grain malformation probability during the Laschamps Event with other sampled time periods. Proportions of malformed Pinus D. grains detected in independent preparations taken from each 150yr sampling interval are shown as black dots (with accompanying sub-scale showing the specific sampling interval). The shaded boxes show the corresponding mean probability estimates obtained after fitting a binomial logistic regression (accounting for overdispersion) to the broader time periods along with their 95% CI intervals (48). The numbers of grains (total and malformed) in each broad period are also given. See Materials and Methods for information on the types of malformations identified, and Fig. S5 for illustrative images of the malformations.

Interpretation

Our results indicate a broad negative linear relationship, extending over the last 65ka, between the amounts of *p*-CA and the ADM. We find very strong evidence (*p-value* < 0.001) that lower geomagnetic field strengths correspond to higher amounts of UV-B absorbing compounds within the grains. The strength of the geodynamo therefore appears to have a direct role in determining the amount of UV-B radiation absorbed by the stratospheric ozone layer before reaching Earth's surface.

In particular, the increased amounts of UV-B absorbing *p*-CA found in our subfossil *Pinus D.* grains provide extremely strong evidence for a substantial increase in UV-B radiation reaching Lake Suigetsu, Japan during the *Laschamps Event*. This increase is persistent, covering at least a 600yr period from 41.3–40.7ka BP. In all four 150yr intervals sampled during this period, the estimated mean *p*-CA levels are uniformly higher than in any other time interval analyzed. We found a 31% increase [95% CI 19-44] in *p*-CA between 41.3–40.7ka BP compared to the period from 1.6–1.0ka BP.

While we did not find evidence for a significant increase in *Pinus D.* grain malformation rates, this should be seen in the context of experiments that indicate extreme UV-B irradiation (>5 times present-day outdoor UV-B flux) is required to induce such changes (*1*). Indeed, the secondary information that *Pinus D.* malformation rates do not change substantially during the *Laschamps* provides an upper bound on the surface UV-B flux during this period.

Additionally, the lack of evidence (*p-value* = 0.63) for a calendar age effect on the *p*-CA content within the subfossil grains indicates biomolecular degradation and/or subfossilization do not affect the biochemical composition of the sporopollenin. This lends strength to the use of this biochemical proxy for reconstructing UV-B irradiance into the past.

Preliminary bounds on surface UV-B flux during the Laschamps Event

Since the dose-response relationship between surface UV-B irradiance and *p*-CA content in *Pinus D.* is not yet established (*30*), we cannot precisely convert our recorded increase in *p*-CA into estimates of absolute UV-B fluxes. We can however provide tentative lower and upper bounds for the mean daily flux over the 41.3–40.7ka BP period.

In terms of a lower bound, greenhouse experiments on *Pinus mugo* cultivars irradiated with a mean UV-B dose of 16.8 kJ m^{-2} day^{-1}_{BE} (BE; biologically effective according to Flint's biological spectral weighting function (*49*)) show a relative increase in *p*-CA of 1.01 (95% CI [0.95-1.07]) compared to controls with no UV-B exposure (see Materials and Methods). The relative increase in *p*-CA of 1.31 (95% CI [1.19-1.4]) that we estimate during 41.3–40.7ka BP compared to 1.6–1.0ka BP is significantly greater than this (as the 95% CI intervals do not overlap). Consequently, from 41.3–40.7ka BP, we suggest that the mean UV-B flux was above the greenhouse dose of 16.8 kJ m^{-2} day^{-1}_{BE}.

To obtain an upper bound, we consider the malformation information. Pollen malformation rates can vary considerably between gymnosperm taxa, but laboratory experiments on the dwarf pine *Pinus mugo* (Columnaris) indicate a UV-B dose of 75 kJ m^{-2} day^{-1}_{BE} induces a step-change in grain malformation probability compared to a no-UV-B control (*1*). This enhanced UV-B dose corresponds to modelled estimates of irradiance during the late-Permian (*4*). Since, we do not observe such a substantial increase in malformations, we infer that during the *Laschamps Event*,

the mean UV-B flux was below this end-Permian 75 kJ m^{-2} day^{-1}_{BE} estimate, when near-total ozone layer collapse was assumed.

Present-day UV-B dosages at Lake Suigetsu, Japan (35˚ 35' N, 135˚ 53' E, 0m amsl) are not available, but USDA estimates (*50*) at a similar latitude and altitude in Raleigh, N. Carolina (35˚ 73' N, 78˚ 68' W, 120m amsl) suggest present-day mean dosages of 14.3 kJ m^{-2} day^{-1}_{BE} during *Pinus* pollen season (March-June) – see Materials and Methods. Our lower bound of 16.8 kJ m^{-2} day^{-1}_{BE} therefore corresponds to a prolonged (lasting >600 years) increase of 18% in surface UV-B irradiance during the *Laschamps* compared to the present day.

To narrow this range further, more understanding is required of the precise quantitative relationship between the amount of *p*-CA generated in *Pinus D.* pollen and the UV-B radiation dose to which the parent plant is exposed.

Implications for Evolution, Ecology and Atmospheric Chemistry

The global climatic, evolutionary, and ecological impacts of geomagnetic excursions and reversals are poorly understood and remain vigorously debated (*7–9*, *13–15*). In addition, the precise mechanisms which might underlie changes in atmospheric chemistry during such events are uncertain (*8*, *9*).

Modelling has presented a range of possible elevated UV-B scenarios based on interactions between geomagnetic field strength, solar activity, and solar storms. These predictions are highly wavelength dependent but suggest that, during a collapse of the geomagnetic field, the greatest (long-lasting) increase in surface UV-B would occur if that weakening were to coincide with a Grand Solar Minimum. Such a combination is modelled to result in an overall 10–15% increase in UV-B radiation in the tropics (*9*). A contemporaneous extreme solar particle event is hypothesized to lead to a higher 30% increase in UV-B but only for 6 years after the event (*8*).

The increases in UV-B indicated by our pollen data, seemingly lasting over 600 years, are of a greater scale than the modelled estimates under the Grand Solar Minimum scenario and of an unusually long duration for such a solar minimum. We do not see evidence for a sudden, sharp spike in the UV-B proxies as hypothesized by the occurrence of an extreme solar particle event (*8*) although the 150yr resolution of our samples may limit our ability to resolve such short-term impacts.

The increase in surface UV-B radiation, lasting for over 600 years, that we infer during the *Laschamps Event* lends support to the hypothesis this period may have been a time of environmental crisis, with potentially deleterious effects upon *Neanderthals* (*9*, *13*). However, to assess global implications, reconstructions from other locations are required. Furthermore, while the Lake Suigetsu record indicates some oscillations in *Pinus D.* abundance over the *Laschamps*, it does not appear palaeomagnetic, or UV-B, variations induced major changes in the lake's ecosystem or led to widespread reproductive failure (see Fig. S2).

This suggests the impacts of paleomagnetic, and UV-B, variations could be more subtle; and indicates a general ecosystem robustness to such elevated UV-B irradiance. Indeed, our findings suggest production of UV-B absorbing compounds was one such protective mechanism allowing these taxa to persist through a period of highly elevated UV-B. This agrees with other studies indicating a suite of plant defence mechanisms that ameliorate exposure to UV-B radiation (*51*, *52*).

Conclusion

Our study provides real-world, empirical evidence for the potential impacts of geomagnetic field strength on UV-B radiation and stratospheric ozone. The strength of the geodynamo has a direct relationship with the amount of UV-B radiation that reaches the Earth's surface. Reductions in geomagnetic field strength will result in damage to the stratospheric ozone layer and consequently lead to increased surface UV-B irradiance. During the *Laschamps Event*, the most recent major geomagnetic excursion, ca. 41ka BP, UV-B radiation at the Earth surface was significantly increased compared to the present day. While the biological impact on ecosystems of changes in UV-B due to geomagnetic variations remains relatively unknown, the geodynamo should be considered as a potential risk for, and driver of, ecological change.

References and Notes

1. J. P. Benca, I. A. P. Duijnstee, C. V Looy, UV-B–induced forest sterility: Implications of ozone shield failure in Earth's largest extinction. *Sci. Adv.* 4, e1700618 (2018).
2. K. J. Willis, K. D. Bennett, H. J. B. Birks, Variability in thermal and UV-B energy fluxes through time and their influence on plant diversity and speciation. *J. Biogeogr.* 36, 1630–1644 (2009).
3. F. Liu, H. Peng, J. E. A. Marshall, B. H. Lomax, B. Bomfleur, M. S. Kent, W. T. Fraser, P. E. Jardine, Dying in the Sun: Direct evidence for elevated UV-B radiation at the end-Permian mass extinction. *Sci. Adv.* 9, eabo6102 (2023).
4. D. J. Beerling, M. Harfoot, B. Lomax, J. A. Pyle, The stability of the stratospheric ozone layer during the end-Permian eruption of the Siberian Traps. *Philosophical Transactions of the Royal Society A: Mathematical, Physical and Engineering Sciences* 365, 1843–1866 (2007).
5. J. E. A. Marshall, J. Lakin, I. Troth, S. M. Wallace-Johnson, UV-B radiation was the Devonian-Carboniferous boundary terrestrial extinction kill mechanism. *Sci. Adv.* 6, eaba0768 (2020).
6. A. F. Bais, G. Bernhard, R. L. McKenzie, P. J. Aucamp, P. J. Young, M. Ilyas, P. Jöckel, M. Deushi, Ozone—climate interactions and effects on solar ultraviolet radiation. *Photochemical & Photobiological Sciences* 18, 602–640 (2019).
7. J. E. T. Channell, L. Vigliotti, The Role of Geomagnetic Field Intensity in Late Quaternary Evolution of Humans and Large Mammals. *Reviews of Geophysics* 57, 709–738 (2019).
8. P. Arsenović, E. Rozanov, I. Usoskin, C. Turney, T. Sukhodolov, K. McCracken, M. Friedel, J. Anet, S. Simić, V. Maliniemi, T. Egorova, M. Korte, H. Rieder, A. Cooper, T. Peter, Global impacts of an extreme solar particle event under different geomagnetic field strengths. *Proceedings of the National Academy of Sciences* 121, e2321770121 (2024).
9. A. Cooper, C. S. M. Turney, J. Palmer, A. Hogg, M. McGlone, J. Wilmshurst, A. M. Lorrey, T. J. Heaton, J. M. Russell, K. McCracken, J. G. Anet, E. Rozanov, M. Friedel, I. Suter, T. Peter, R. Muscheler, F. Adolphi, A. Dosseto, J. T. Faith, P. Fenwick, C. J. Fogwill, K. Hughen, M. Lipson, J. Liu, N. Nowaczyk, E. Rainsley, C. Bronk Ramsey, P. Sebastianelli, Y. Souilmi, J. Stevenson, Z. Thomas, R. Tobler, R. Zech, A global environmental crisis 42,000 years ago. *Science* 371, 811 – 818 (2021).
10. A. Mukhopadhyay, S. Panovska, R. Garvey, M. W. Liemohn, N. Ganjushkina, A. Brenner, I. Usoskin, M. Balikhin, D. T. Welling, Wandering of the auroral oval 41,000 years ago. *Sci. Adv.* 11 (2025).
11. I. Lascu, J. M. Feinberg, J. A. Dorale, H. Cheng, R. L. Edwards, Age of the Laschamp excursion determined by U-Th dating of a speleothem geomagnetic record from North America. *Geology* 44, 139–142 (2016).
12. N. Bonhommet, J. Babkine, Sur la presence d'aimentation inverse dans la Chaine des Puys. *Comptes rendus hebdomadaires des séances de l'Académie des sciences Ser. B* 264, 92–94 (1967).
13. J.-P. Valet, H. Valladas, The Laschamp-Mono lake geomagnetic events and the extinction of Neanderthal: a causal link or a coincidence? *Quat. Sci. Rev.* 29, 3887–3893 (2010).
14. A. Picin, S. Benazzi, R. Blasco, M. Hajdinjak, K. M. Helgen, J.-J. Hublin, J. Rosell, P. Skoglund, C. Stringer, S. Talamo, Comment on "A global environmental crisis 42,000 years ago." *Science* 374, eabi8330 (2024).
15. J. Hawks, Comment on "A global environmental crisis 42,000 years ago." *Science* 374, eabh1878 (2024).

16. D. Gubbins, A. L. Jones, C. C. Finlay, Fall in Earth's Magnetic Field Is Erratic. *Science* 312, 900 – 902 (2006).
17. T. J. Heaton, E. Bard, C. Bronk Ramsey, M. Butzin, P. Köhler, R. Muscheler, P. J. Reimer, L. Wacker, Radiocarbon: A key tracer for studying Earth's dynamo, climate system, carbon cycle, and Sun. *Science* 374, eabd7096 (2021).
18. S. Maffei, J. W. B. Eggington, P. W. Livermore, J. E. Mound, S. Sanchez, J. P. Eastwood, M. P. Freeman, Climatological predictions of the auroral zone locations driven by moderate and severe space weather events. *Sci. Rep.* 13, 779 (2023).
19. J. M. Bowler, H. Johnston, J. M. Olley, J. R. Prescott, R. G. Roberts, W. Shawcross, N. A. Spooner, New ages for human occupation and climatic change at Lake Mungo, Australia. *Nature* 421, 837–840 (2003).
20. A. Cooper, C. Turney, K. A. Hughen, B. W. Brook, H. G. McDonald, C. J. A. Bradshaw, Abrupt warming events drove Late Pleistocene Holarctic megafaunal turnover. *Science* 349, 602–606 (2015).
21. T. Higham, K. Douka, R. Wood, C. B. Ramsey, F. Brock, L. Basell, M. Camps, A. Arrizabalaga, J. Baena, C. Barroso-Ruíz, C. Bergman, C. Boitard, P. Boscato, M. Caparrós, N. J. Conard, C. Draily, A. Froment, B. Galván, P. Gambassini, A. Garcia-Moreno, S. Grimaldi, P. Haesaerts, B. Holt, M.-J. Iriarte-Chiapusso, A. Jelinek, J. F. Jordá Pardo, J.-M. Maíllo-Fernández, A. Marom, J. Maroto, M. Menéndez, L. Metz, E. Morin, A. Moroni, F. Negrino, E. Panagopoulou, M. Peresani, S. Pirson, M. de la Rasilla, J. Riel-Salvatore, A. Ronchitelli, D. Santamaria, P. Semal, L. Slimak, J. Soler, N. Soler, A. Villaluenga, R. Pinhasi, R. Jacobi, The timing and spatiotemporal patterning of Neanderthal disappearance. *Nature* 512, 306–309 (2014).
22. M. Aubert, R. Lebe, A. A. Oktaviana, M. Tang, B. Burhan, Hamrullah, A. Jusdi, Abdullah, B. Hakim, J. Zhao, I. M. Geria, P. H. Sulistyarto, R. Sardi, A. Brumm, Earliest hunting scene in prehistoric art. *Nature* 576, 442–445 (2019).
23. F. Saltré, M. Rodríguez-Rey, B. W. Brook, C. N. Johnson, C. S. M. Turney, J. Alroy, A. Cooper, N. Beeton, M. I. Bird, D. A. Fordham, R. Gillespie, S. Herrando-Pérez, Z. Jacobs, G. H. Miller, D. Nogués-Bravo, G. J. Prideaux, R. G. Roberts, C. J. A. Bradshaw, Climate change not to blame for late Quaternary megafauna extinctions in Australia. *Nat. Commun.* 7, 10511 (2016).
24. S. Dasari, G. Paris, J. Charreau, J. Savarino, Sulfur-isotope anomalies recorded in Antarctic ice cores as a potential proxy for tracing past ozone layer depletion events. *PNAS Nexus* 1, pgac170 (2022).
25. P. E. Jardine, W. T. Fraser, B. H. Lomax, M. A. Sephton, T. M. Shanahan, C. S. Miller, W. D. Gosling, Pollen and spores as biological recorders of past ultraviolet irradiance. *Sci. Rep.* 6, 39269 (2016).
26. P. E. Jardine, W. T. Fraser, W. D. Gosling, C. N. Roberts, W. J. Eastwood, B. H. Lomax, Proxy reconstruction of ultraviolet-B irradiance at the Earth's surface, and its relationship with solar activity and ozone thickness. *Holocene* 30, 155–161 (2019).
27. J. Rozema, A. J. Noordijk, R. A. Broekman, A. van Beem, B. M. Meijkamp, N. V. J. de Bakker, J. W. M. van de Staaij, M. Stroetenga, S. J. P. Bohncke, M. Konert, S. Kars, H. Peat, R. I. L. Smith, P. Convey, (Poly)phenolic compounds in pollen and spores of Antarctic plants as indicators of solar UV-B – A new proxy for the reconstruction of past solar UV-B? *Plant Ecol.* 154, 9–26 (2001).
28. K. J. Willis, A. Feurdean, H. J. B. Birks, A. E. Bjune, E. Breman, R. Broekman, J.-A. Grytnes, M. New, J. S. Singarayer, J. Rozema, Quantification of UV-B flux through time using UV-B-absorbing compounds contained in fossil Pinus sporopollenin. *New Phytologist* 192, 553–560 (2011).
29. B. H. Lomax, W. T. Fraser, M. A. Sephton, T. V Callaghan, S. Self, M. Harfoot, J. A. Pyle, C. H. Wellman, D. J. Beerling, Plant spore walls as a record of long-term changes in ultraviolet-B radiation. *Nat. Geosci.* 1, 592–596 (2008).
30. A. W. R. Seddon, D. Festi, M. Nieuwkerk, R. Gya, B. Hamre, L. C. Krüger, S. A. H. Östman, T. M. Robson, Pollen-chemistry variations along elevation gradients and their implications for a proxy for UV-B radiation in the plant-fossil record. *Journal of Ecology* 109, 3060–3073 (2021).
31. A. W. R. Seddon, M. Jokerud, T. Barth, H. J. B. Birks, L. C. Krüger, V. Vandvik, K. J. Willis, Improved quantification of UV-B absorbing compounds in Pinus sylvestris L. pollen grains using an internal standard methodology. *Rev. Palaeobot. Palynol.* 247, 97–104 (2017).
32. A. W. R. Seddon, D. Festi, T. M. Robson, B. Zimmermann, Fossil pollen and spores as a tool for reconstructing ancient solar-ultraviolet irradiance received by plants: an assessment of prospects and challenges using proxy-system modelling. *Photochemical & Photobiological Sciences* 18, 275–294 (2019).
33. C. Bronk Ramsey, T. J. Heaton, G. Schlolaut, R. A. Staff, C. L. Bryant, A. Brauer, H. F. Lamb, M. H. Marshall, T. Nakagawa, Reanalysis of the Atmospheric Radiocarbon Calibration Record from Lake Suigetsu, Japan. *Radiocarbon* 62, 989–999 (2020).

34. T. Nakagawa, H. Kitagawa, Y. Yasuda, P. E. Tarasov, K. Nishida, K. Gotanda, Y. Sawai, Y. R. C. P. Members1, Asynchronous Climate Changes in the North Atlantic and Japan During the Last Termination. *Science* 299, 688–691 (2003).
35. J. Gao, M. Korte, S. Panovska, Z. Rong, Y. Wei, Geomagnetic field shielding over the last one hundred thousand years. *J. Space Weather Space Clim.* 12 (2022).
36. S. Panovska, M. Korte, C. G. Constable, One Hundred Thousand Years of Geomagnetic Field Evolution. *Reviews of Geophysics* 57, 1289–1337 (2019).
37. G. Schlolaut, R. A. Staff, A. Brauer, H. F. Lamb, M. H. Marshall, C. Bronk Ramsey, T. Nakagawa, An extended and revised Lake Suigetsu varve chronology from ∼50 to ∼10 ka BP based on detailed sediment micro-facies analyses. *Quat. Sci. Rev.* 200, 351–366 (2018).
38. V. C. Smith, R. A. Staff, S. P. E. Blockley, C. Bronk Ramsey, T. Nakagawa, D. F. Mark, K. Takemura, T. Danhara, Identification and correlation of visible tephras in the Lake Suigetsu SG06 sedimentary archive, Japan: chronostratigraphic markers for synchronising of east Asian/west Pacific palaeoclimatic records across the last 150 ka. *Quat. Sci. Rev.* 67, 121–137 (2013).
39. M. Hyodo, T. Nakagawa, H. Matsushita, I. Kitaba, K. Yamada, S. Tanabe, B. Bradák, M. Miki, D. McLean, R. A. Staff, V. C. Smith, P. G. Albert, C. Bronk Ramsey, A. Yamasaki, J. Kitagawa, G. Schlolaut, K. Gotanda, K. Tsumura, K. Inagawa, K. Kumazawa, H. Abe, S. Sugo, K. Takahashi, A. Kitamura, S. 2014 Project, Intermittent non-axial dipolar-field dominance of twin Laschamp excursions. *Commun. Earth Environ.* 3, 79 (2022).
40. R. Leonhardt, K. Fabian, M. Winklhofer, A. Ferk, C. Laj, C. Kissel, Geomagnetic field evolution during the Laschamp excursion. *Earth Planet. Sci. Lett.* 278, 87–95 (2009).
41. C. B. Foster, S. A. Afonin, Abnormal pollen grains: an outcome of deteriorating atmospheric conditions around the Permian–Triassic boundary. *J. Geol. Soc. London.* 162, 653–659 (2005).
42. J. P. Benca, I. A. P. Duijnstee, C. V Looy, Fossilized pollen malformations as indicators of past environmental stress and meiotic disruption: insights from modern conifers. *Paleobiology* 48, 677–710 (2022).
43. S. Lindström, H. Sanei, B. van de Schootbrugge, G. K. Pedersen, C. E. Lesher, C. Tegner, C. Heunisch, K. Dybkjær, P. M. Outridge, Volcanic mercury and mutagenesis in land plants during the end-Triassic mass extinction. *Sci. Adv.* 5, eaaw4018 (2019).
44. B. R. Murphy, F. J. G. Mitchell, An association between past levels of ozone column depletion and abnormal pollen morphology in the model angiosperm Arabidopsis thaliana L. *Rev. Palaeobot. Palynol.* 194, 12–20 (2013).
45. H. Visscher, C. V Looy, M. E. Collinson, H. Brinkhuis, J. H. A. van Konijnenburg-van Cittert, W. M. Kürschner, M. A. Sephton, Environmental mutagenesis during the end-Permian ecological crisis. *Proceedings of the National Academy of Sciences* 101, 12952–12956 (2004).
46. N. De Storme, D. Geelen, The impact of environmental stress on male reproductive development in plants: biological processes and molecular mechanisms. *Plant Cell Environ.* 37, 1–18 (2014).
47. P. W. Barnes, M. A. Tobler, K. Keefover-Ring, S. D. Flint, A. E. Barkley, R. J. Ryel, R. L. Lindroth, Rapid modulation of ultraviolet shielding in plants is influenced by solar ultraviolet radiation and linked to alterations in flavonoids. *Plant Cell Environ.* 39, 222–230 (2016).
48. D. A. Williams, Extra-Binomial Variation in Logistic Linear Models. *J. R. Stat. Soc. Ser. C Appl. Stat.* 31, 144–148 (1982).
49. S. D. Flint, M. M. Caldwell, A biological spectral weighting function for ozone depletion research with higher plants. *Physiol. Plant.* 117, 137–144 (2003).
50. D. S. Bigelow, J. R. Slusser, A. F. Beaubien, J. H. Gibson, The USDA Ultraviolet Radiation Monitoring Program. *Bull. Am. Meteorol. Soc.* 79, 601–615 (1998).
51. P. W. Barnes, T. M. Robson, M. A. Tobler, I. N. Bottger, S. D. Flint, "Plant responses to fluctuating UV environments." in *UV-B Radiation and Plant Life: Molecular Biology to Ecology* (CABI, UK, 2017), pp. 72–89.
52. P. W. Barnes, T. M. Robson, P. J. Neale, C. E. Williamson, R. G. Zepp, S. Madronich, S. R. Wilson, A. L. Andrady, A. M. Heikkilä, G. H. Bernhard, A. F. Bais, R. E. Neale, J. F. Bornman, M. A. K. Jansen, A. R. Klekociuk, J. Martinez-Abaigar, S. A. Robinson, Q.-W. Wang, A. T. Banaszak, D.-P. Häder, S. Hylander, K. C. Rose, S.-Å. Wängberg, B. Foereid, W.-C. Hou, R. Ossola, N. D. Paul, J. E. Ukpebor, M. P. S. Andersen, J. Longstreth, T. Schikowski, K. R. Solomon, B. Sulzberger, L. S. Bruckman, K. K. Pandey, C. C. White, L. Zhu, M. Zhu, P. J. Aucamp, J. B. Liley, R. L. McKenzie, M. Berwick, S. N. Byrne, L. M. Hollestein, R. M. Lucas, C. M. Olsen, L. E. Rhodes, S. Yazar, A. R. Young, Environmental effects of

stratospheric ozone depletion, UV radiation, and interactions with climate change: UNEP Environmental Effects Assessment Panel, Update 2021. *Photochemical & Photobiological Sciences* 21, 275–301 (2022).

53. C. Bronk Ramsey, R. A. Staff, C. L. Bryant, F. Brock, H. Kitagawa, J. van der Plicht, G. Schlolaut, M. H. Marshall, A. Brauer, H. F. Lamb, R. L. Payne, P. E. Tarasov, T. Haraguchi, K. Gotanda, H. Yonenobu, Y. Yokoyama, R. Tada, T. Nakagawa, A Complete Terrestrial Radiocarbon Record for 11.2 to 52.8 kyr B.P. *Science (1979).* 338, 370 – 374 (2012).
54. P. G. Albert, V. C. Smith, T. Suzuki, D. McLean, E. L. Tomlinson, Y. Miyabuchi, I. Kitaba, D. F. Mark, H. Moriwaki, T. Nakagawa, Geochemical characterisation of the Late Quaternary widespread Japanese tephrostratigraphic markers and correlations to the Lake Suigetsu sedimentary archive (SG06 core). *Quat. Geochronol.* 52, 103–131 (2019).
55. C. Laj, J. E. T. Channell, "5.10 - Geomagnetic Excursions" in *Treatise on Geophysics (Second Edition)*, G. Schubert, Ed. (Elsevier, Oxford, 2015; https://www.sciencedirect.com/science/article/pii/B9780444538024001044), pp. 343–383.
56. U. Bleil, G. Gard, Chronology and correlation of Quaternary magnetostratigraphy and nannofossil biostratigraphy in Norwegian-Greenland Sea sediments. *Geologische Rundschau* 78, 1173–1187 (1989).
57. N. R. Nowaczyk, T. W. Frederichs, Geomagnetic events and relative palaeointensity variations during the past 300 ka as recorded in Kolbeinsey Ridge sediments, Iceland Sea: indication for a strongly variable geomagnetic field. *International Journal of Earth Sciences* 88, 116–131 (1999).
58. E. Thellier, O. Thellier, Sur l'intensité du champ magnétique terrestre, en France, trois siècles avant les premières mesures directes. Application, au problème de la désaimantation du globe. *C. R. Acad. Sci. Paris* 214, 382–384 (1942).
59. N. R. Nowaczyk, U. Frank, J. Kind, H. W. Arz, A high-resolution paleointensity stack of the past 14 to 68 ka from Black Sea sediments. *Earth Planet. Sci. Lett.* 384, 1–16 (2013).
60. W. T. Fraser, J. S. Watson, M. A. Sephton, B. H. Lomax, G. Harrington, W. D. Gosling, S. Self, Changes in spore chemistry and appearance with increasing maturity. *Rev. Palaeobot. Palynol.* 201, 41–46 (2014).
61. F. Muthreich, " New methods in Palaeopalynology: Classification of pollen through pollen chemistry. ," thesis, Uni. Bergen PhD thesis. (2021).
62. T. Wang, B. A. Bell, W. J. Fletcher, P. A. Ryan, R. A. Wogelius, Influence of common palynological extraction treatments on ultraviolet absorbing compounds (UACs) in sub-fossil pollen and spores observed in FTIR spectra. *Front. Ecol. Evol.* 11 (2023).
63. P. Blokker, D. Yeloff, P. Boelen, R. A. Broekman, J. Rozema, Development of a Proxy for Past Surface UV-B Irradiation: A Thermally Assisted Hydrolysis and Methylation py-GC/MS Method for the Analysis of Pollen and Spores. *Anal. Chem.* 77, 6026–6031 (2005).
64. R Core Team, R: A Language and Environment for Statistical Computing. [Preprint] (2024). https://www.R-project.org/.
65. E. C. Fieller, Some Problems in Interval Estimation. *Journal of the Royal Statistical Society. Series B (Methodological)* 16, 175–185 (1954).
66. P. A. Hochuli, E. Schneebeli-Hermann, G. Mangerud, H. Bucher, Evidence for atmospheric pollution across the Permian-Triassic transition. *Geology* 45, 1123–1126 (2017).
67. W. M. Kürschner, S. J. Batenburg, L. Mander, Aberrant Classopollis pollen reveals evidence for unreduced (2n) pollen in the conifer family Cheirolepidiaceae during the Triassic–Jurassic transition. *Proceedings of the Royal Society B: Biological Sciences* 280, 20131708 (2013).
68. J. Gravendyck, M. Schobben, J. B. Bachelier, W. M. Kürschner, Macroecological patterns of the terrestrial vegetation history during the end-Triassic biotic crisis in the central European Basin: A palynological study of the Bonenburg section (NW-Germany) and its supra-regional implications. *Glob. Planet. Change* 194, 103286 (2020).

Acknowledgments: We thank K Krüger, V Smith, and S Tobias for productive discussions which improved our manuscript. TJH would like to thank A Al-Mukhtar, S Daniels, and all the staff in Firth 8 and 9 of the Northern General Hospital, Sheffield for looking after him during a period of ill health coinciding with elements of this work.

Funding:

NERC Global Partnerships Seedcorn Fund NE/Y002652/1 (TJH, AWRS, TN) and Research Council of Norway QUEST-UV Reference: 324670 (AWRS).

Author contributions:

Conceptualization: TJH, AWRS, EB

Methodology: TJH, AWRS, EW-R, LCK, CSL, TMR, TN

Investigation: EW-R, LCK, TJH, AWRS, CSL, AM, TMR, TN

Visualization: TJH

Funding acquisition: TJH, AWRS, TN

Project administration: TJH, AWRS

Supervision: TJH, AWRS, LCK, CSL

Writing – original draft: TJH, AWRS

Writing – review & editing: All

Competing interests: Authors declare that they have no competing interests.

Data and materials availability: All data, code, and materials used in the analysis is available at https://github.com/TJHeaton/Increased_UVB_Laschamps. Measurements of present-day surface UV-B irradiance at Raleigh, N. Carolina are available from the USDA at https://uvb.nrel.colostate.edu/UVB/

Supplementary Materials

Materials and Methods:

Lake Suigetsu Sediment Core

Lake Suigetsu is a tectonic lake, situated close to the Sea of Japan coast at Wakasa Bay, Honshu, central Japan (35˚ 35' N, 135˚ 53' E, see Figs. S1 and S2). The sediment sequence we used for sampling ('SG06') was obtained from a coring expedition in 2006 and extends back approximately 150ka. Lake Suigetsu contains extremely well-preserved annual laminations (varves) due to the location's marked seasonality, and the lake hydrology which creates anoxic (deoxygenated) benthic water conditions preventing bioturbation by basal-dwelling organisms. Coupled with >800 radiocarbon determinations, these varves permit a highly-precise and robust calendar age chronology for the sediment sequence extending back to 55ka (*33*, *53*). Beyond this, annual varves continue in the Suigetsu core until ~70ka. Throughout, the chronology is bolstered by the additional discovery of tephra layers (volcanic ash) which are geochemically correlated to dated eruptions (*38*, *54*), providing calendar age estimates which can be combined with the varves and radiocarbon determinations.

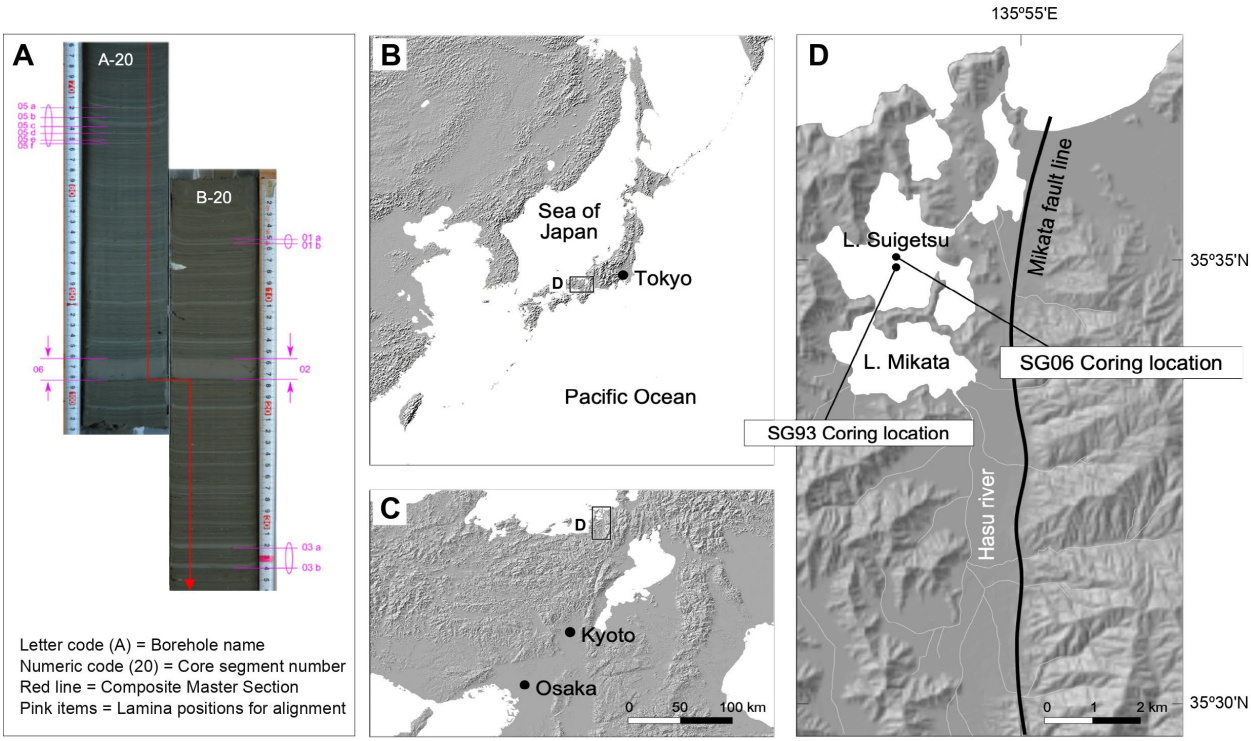

Fig. S1: Lake Suigetsu Sediment Core. Panel A – Lake Suigetsu's annual layering identifiable as varves (in combination with ^{14}C determinations and tephra horizons, enable construction of a highly-precise core chronology dating back to ~70ka. Panel B, C, and D – Location of Lake Suigetsu in Japan.

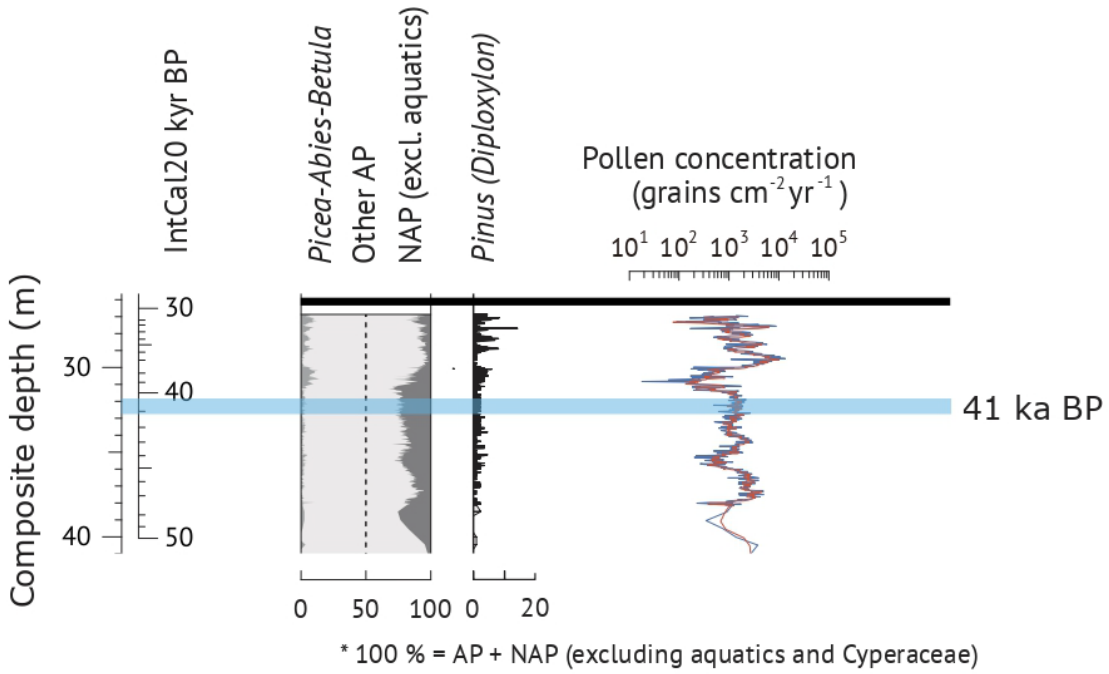

Fig. S2: Lake Suigetsu summary pollen diagram spanning 50 – 30ka BP, including Arboreal Pollen (AP) and Non-Arboreal Pollen (NAP) percentages, Pinus (Diploxylon) percentages and the total pollen concentration. The calendar scale refers to (IntCal20). The Laschamps Geomagnetic Reversal is highlighted. Note the relative stable variations in AP:NAP ratios, Pinus D. percentages and pollen concentrations over the period of interest.

Experimental Design of Sampling

We selected five time periods over the past 70ka for sampling aiming to cover the possible design space. Both the geomagnetic field strength at the point that the pollen grains were formed and the calendar age of the subfossil grains were considered as explanatory variables for our two UV-B radiation measures.

We included the two periods of lowest dipole moment during this 70ka window: the *Laschamps Event* around 41ka BP (*55*) and the *Norwegian-Greenland Sea* excursion around 65ka BP (*56*, *57*). We also considered the two periods with the highest geomagnetic field strengths around 1ka and 53ka BP (*36*).

The calendar age of the subfossil grains is predominantly considered as a nuisance variable (it is not of direct/primary interest). However, its inclusion should allow us to account for potential biomolecular degradation of the sporopollenin over time in our analyses.

The five sampled time periods are shown Fig. S3. There is low collinearity (correlation = -0.42) between the two explanatory variables. This low collinearity increases our ability/power to precisely estimate the individual regression coefficients for each variable within the later UV-B analyses.

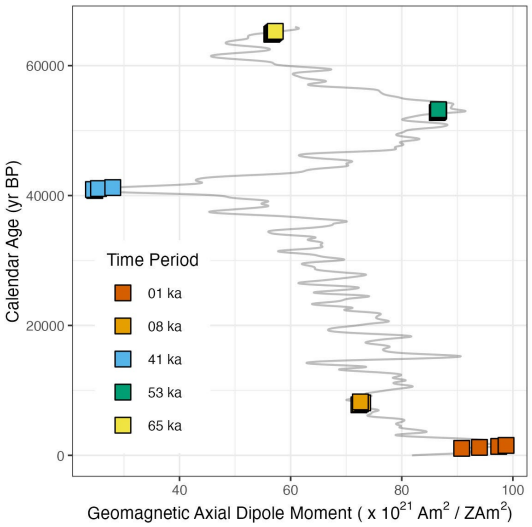

Fig. S3 Experimental/Sampling Design. Five core sections of the Lake Suigetsu record were sampled for Pinus D. pollen. These periods were selected to cover a range of both calendar age and geomagnetic field strength. Each period was then subdivided into four contiguous 150yr sections, resulting in 20 sampling periods overall.

Choice of GGF100ka ADM Geomagnetic Reconstruction

A range of paleomagnetic reconstructions are available. Global compilations of (virtual) axial dipole and non-dipole moments (*35*, *36*) are based upon combinations/stacks of multiple records in different locations combined through modelling. Paleomagnetic estimates are also available from individual locations including a reconstruction using the Lake Suigetsu sediment itself (*39*). These estimates represent the local expression of Earth's magnetic variations in both intensity (dipole and non-dipole) and direction (declination and inclination).

The overall level of shielding from incoming solar and galactic cosmic rays that the geomagnetic field provides (and hence the potential impact on ozone and surface UV-B levels) is dependent upon the overall dipole power (*35*) rather than its direction. During a geomagnetic excursion such as the *Laschamps Event*, dynamic non-dipolar components may lead to considerable deviations among predicted paleomagnetic records at different locations (*40*). Consequently, localised records may be unreliable in estimating overall dipole power during such events. We therefore use the global GGF100ka ADM reconstruction (*36*) as our explanatory variable to understand the potential effect of the geomagnetic field on surface UV-B.

Furthermore, localised paleomagnetic records obtained from sediment are affected by various problems. Reconstruction of the intensity of the geomagnetic field can be achieved by analysing various archives. The thermoremanent magnetization of volcanic rocks and archaeological archives such as baked clays, provide absolute intensities of the geomagnetic field. However, a particular measurement represents the local and instantaneous field including its deviations from the global dipolar field (*58*). By contrast, the remanent magnetization of marine and lacustrine sediments only provides a relative estimation of the geomagnetic field, which needs to be normalized to the present-day dipole intensity or absolute values for past periods based on volcanic or archaeological archives (*59*). This can introduce biases. The other pitfall of sediments is that the geomagnetic field is fossilized at some depth below the sediment-water interface (lock-in depth), leading to stratigraphic and dating uncertainties. These challenges are tentatively discussed in the context of Lake Suigetsu sediments (*39*).

Varved sediments such as those from Lake Suigetsu present many advantages (notably a high stratigraphic and temporal resolution and a lack of bioturbation) in comparison to non-varved sediments. However, this may come at the expense of additional pitfalls when used for paleomagnetic reconstruction (e.g., seasonal and short-term variations of detrital or authigenic magnetic minerals, more local and non-dipolar magnetic variations registered at high resolution).

Individual sediment cores are therefore best considered as providing continuous records that average short-term local non-dipole deviations, by contrast to values given by, e.g., volcanic rocks. The most reliable estimates of the global axial dipole moment likely arise by combining both types of record (such as GGF100ka).

Estimation of Expected Paleomagnetic Field Strength

The expected geomagnetic axial dipole moment was estimated for each 150yr section sampled. The calendar age uncertainty in the Lake Suigetsu chronology (*33*) was incorporated in the calculation of these expected ADM values. This calendar age uncertainty varies from $\pm$ 12 years (1σ) at 1ka BP, up to $\pm$ 2600 years (1σ) at 65ka BP when radiocarbon samples are no longer available. Uncertainty in the calendar scale of the GGF100ka reconstruction was not incorporated as it is not accompanied by such an estimate. However, our five selected broad sampling periods do not exhibit large changes in ADM values over the plausible range of GGF100ka calendar uncertainties (see Fig. 1). Furthermore, the timing of the *Laschamps Event* in Lake Suigetsu is aligned with the timing in the GGF100ka reconstruction (*33*, *39*). Hence our analyses remain robust to any calendar age uncertainty in the GGF100ka reconstruction.

Sporopollenin-based Biomarkers for UV-B Radiation

The outer walls (exines) of pollen grains are formed of the complex biopolymer, sporopollenin. Sporopollenin is partly composed of UV-B absorbing phenolic compounds (e.g., *para*-coumaric and ferulic acids), which are found in increased concentrations in pollen grains whose parent plant has been exposed to higher doses of UV-B radiation (*25–28*). Since sporopollenin is chemically stable over long time periods and is resistant to corrosion in lakes and bogs (*60*), analysis of the chemical composition of pollen grains provides a tool to reconstruct surface UV-B radiation in the past (*25–30*, *32*).

The UV-B absorbing compound *p*-CA is produced as part of the phenylpropanoid pathway and is an integral part of the complex biopolymer sporopollenin. Although a building block for numerous other compounds in the plant, the aromatic ring within the sporopollenin efficiently absorbs UV-B radiation and is thought to act as a protective screen for the genetic material found within the pollen grain. Although dose-response relationships for the abundance of p-CA as a function of received biologically effective UV-B irradiation have not yet been established (*30*), an increased abundance of UV-B absorbing compounds has been identified in a number of fossil sequences across various taxa (*3*, *25*, *26*, *28*, *29*). This increased content of UV-B absorbing compounds has been inferred to reflect changes in the total amount of UV-B radiation received at the Earth's surface.

Our biochemical analyses are performed using pyrolysis-Gas Chromatography-Mass Spectrometry (py-GC-MS). This allows for identification and absolute quantification of the *p*-CA in relation to reference standards (*31*).

Pollen Extraction

Sampling and Preparation

We sampled 150-year sections (as described in Fig. 1) from continuous L-channels of the Lake Suigetsu sediment cores. These sediment samples were processed using established methods to produce concentrated pollen residues (*31*, *61*). Sediments were manually disaggregated by shaking in 50 ml centrifuge tubes filled with distilled water. Prior to density separation, suspended clay residues were removed (poured off) following 7–10 rounds of centrifugation in distilled water, at 3000 rpm. The pollen grains were then concentrated (floated off) through density separation using the inert salt, sodium polytungstate at 1.42 g cm^{-3}. This approach, using no chemical digestion procedures on the pollen or sediments, has the advantage of using minimal physical or chemical treatments on the fossil-pollen samples, hence mitigating risk of degrading samples during preparation (*62*).

Preparation for GC-MS analysis

The concentrated pollen residues were transferred to an individual well on 3-well concavity slide (Electron Microscopy Sciences, Cat.#71878-04) in distilled water. The number of malformed *Pinus D.* grains present on the slides and phenotypically normal *Pinus D.* pollen grains were then counted using a Zeiss AXIO.Vert A1 inverted microscope (see later section and Fig. S5).

Phenotypically normal (non-malformed) *Pinus D.* grains were then manually extracted from the same microscope slide and transferred to a 30µl microvial (GL Sciences- DMI sample insert: 2406-1010) using a drawn-out Pasteur mouth pipette (*31*). The malformed *Pinus D.* grains were not considered for sporopollenin analysis so as not to bias any biomolecular inference. For each depth sampled, twenty depths in total, we generated at least three replicates each containing 100 *Pinus* grains (> 300 *Pinus* grains isolated per depth in total). The replicates were then analysed using py-GC-MS to measure the levels of UV-B absorbing *p*-CA within the sporopollenin. Three replicates had fewer than 100 pollen grains because of low pollen concentrations. We rescaled these intensities to represent 100 grains in post processing, based on the fact that the relationship between integrated abundance (counts per minute) and the number of pollen grains is linear in our py-GC-MS measurements.

Pyrolysis Gas Chromatography Mass Spectrometry

Quantification of *p*-CA by GC/MS followed a modified protocol developed in previous work (*31*, *63*). Pollen samples were hydrolysed to dissolve the compounds in the pollen grains. 4µl of a 1:10 dilution of 30% tetramethylammonium hydroxide (TMAH): methanol (MeOH) was added to the microvials containing the pollen. The microvials were then centrifuged for ten seconds, left at room temperature for 30 minutes, and finally placed in an oven of 70°C for two hours. An internal standard (1µl solution of 4-hydroxy-3-methoxybenzoic (vanillic) acid, Sigma Aldrich, ≥ 97,0%) was added to each sample.

An Agilent 8860 GC with an Agilent 5975 Mass Selective Detector (MSD) was used for all analyses. The GC system was equipped with an Optic-4 PTV-injector (ATAS GL, Veldhoven, The Netherlands) and PAL Combi robotic autosampler (ATAS GL). The PTV supplies the helium carrier gas by an electronic gas control unit. The column of the GC was An HP - Ultra 25 m x 0.2 mm (internal diameter) column with a 0.33 µm film. The carrier gas had a column flow set to 1.0 ml/min^{-1}, and the split flow was set to 20 ml/min^{-1}. For pyrolysis, the temperature was set to rise from 40°C to 600°C at maximum ramp rate and held for 30 seconds. The GC oven had a temperature from 40°C (held for six minutes) to 130°C at a rate of 15°C min^{-1} , then to 250°C at 8°C min^{-1}, to 300°C at 15°C min^{-1} and then held for 1.5 minutes at 300°C. Data acquisition was run in scan mode to monitor a mass range between m/z 50 and 550 at 2.94 scans s^{-1}.

To quantify *p*-CA in the pollen samples we used an external calibration series consisting of a series of *P. uncinata* pollen taken from Vallter, Pyrenees in 2019, with known numbers of pollen grains (50, 150, 300 and 450 pollen grain samples in each sample). This calibration series was run at the start of each batch of 16 sediment core replicate samples, we used these batch-specific calibration curves to convert our subfossil pollen estimates into estimated numbers of pollen grains from our standard. We also ran a series of external calibration samples based on analytical standards with known concentrations of *p*-CA. We combined all our pollen calibration series with these external analytical standards so that our fossil pollen estimates could be quantified in ng-grain^{-1}. Quantification of *p*-CA was based on the ratio of two ions (i161: i196), following addition of a vanillic acid internal standard into each sample, which increases precision in pollen chemistry measurements (*31*).

Statistical Regression Analysis of *p*-CA Levels

All analyses were performed using R (*64*) and code to reproduce them is available on Github (https://github.com/TJHeaton/Increased_UVB_Laschamps).

Linear Regression on p-CA Levels

We fitted a linear model to the amount of UV-B absorbing *p*-CA (ng grain^{-1}) identified in the 72 replicates across the twenty sampled periods. The expected geomagnetic ADM (*36*) over the 150yr time interval in which the sampled pollen was formed (ZAm^2) and the calendar age of the subfossil pollen (yr BP) were used as explanatory variables. The inclusion of the calendar age of the sampled pollen allows for its potential biomolecular degradation over time. For the i^{th} sample, at calendar age θ_i, we model:

$$y_i = \beta_0 + \beta_1 x_i + \beta_2 \theta_i + \epsilon_i \qquad \text{for } i = 1, \ldots, 20.$$

Here y_i is the amount of *p*-CA (ng grain^{-1}) in the i^{th} sample, x_i is the expected ADM at the time θ_i of grain formation, and $\epsilon_i \sim N(0, \sigma_i^2)$ are independent with σ_i^2 unknown and estimated from the sample replicates. A summary of the model can be found in Table S1, with residual plots (for

model checking) in Fig. S4. These residuals indicate an overall satisfactory fit for the model, although we do see some suggestion of heavy positive tails with a few replicates that report particularly high values of *p*-CA compared with that expected (in particular, two replicates at 53ka BP). We do not see evidence for heteroskedasticity, although the replicates from the 8ka BP period do appear to have slightly less spread than those in the other time periods.

	Regression Coefficient			
Explanatory Variable	Estimate	S.E.	95% CI	p-value
Intercept	5.47×10^{-1}	2.61×10^{-2}	$[4.95, 5.99] \times 10^{-1}$	$< 2 \times 10^{-16}$
Geomagnetic ADM (ZAm^2)	-1.73×10^{-3}	2.88×10^{-4}	$[-2.31, -1.16] \times 10^{-3}$	8.07×10^{-8}
Calendar Age (yr BP)	-1.53×10^{-7}	3.16×10^{-7}	$[-4.78, 7.84] \times 10^{-7}$	0.629
	Residual Standard Error (69 df)		0. 05933	
	R^2		0.3956	
	F-statistic (2 and 69 df)		22.58	2.86×10^{-8}

Table S1 Summary of p-CA linear model considering geomagnetic dipole moment and grain calendar age as explanatory variables.

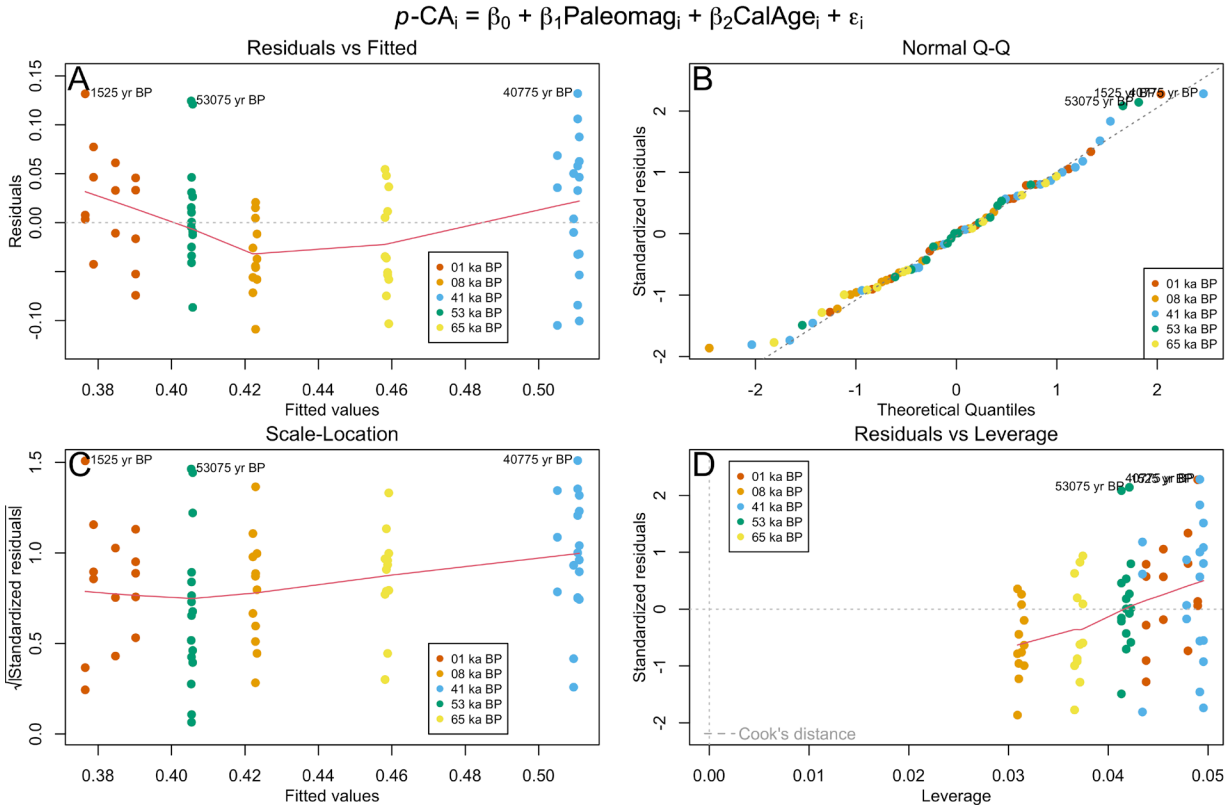

Fig. S4 Linear Model Diagnostic Plots. Panel A – Tukey-Anscombe plot. Panel B – QQ plot. Panel C – Scale-Location plot, Panel D: Residuals vs Leverage plot.

Analysis of Relative Increase in p-CA during the Laschamps Event

To estimate the relative increase in the amount of *p*-CA (ng grain^{-1}) within the *Pinus D.* grains during the *Laschamps Event* we considered the observed levels obtained in all 72 independent (150 yr-interval) samples prepared from the Lake Suigetsu sediment record. The measurements were classified according to the broad 600yr time period from which they arose (i.e., either from 1.3, 8, 41, 53, or 65ka BP). There were 18 samples from the *Laschamps Event* (covering the independent intervals 41300–41150, 41150–41000, 41000–40850, and 40850–40700 yrs BP) as shown in Fig. 1.

Each sampled observation of the *p*-CA level, y_i, was assumed to arise from a $N(\mu_j, \tau_j^2)$ where j is the overall time period (i.e., 1.3, 8, 41, 53, or 65ka BP) to which sample i belonged. Bartlett's test provided no evidence against homogeneity of variance in the observed mean *p*-CA values across the five broad time periods (K^2 statistic = 4.92, df = 4, *p-value* = 0.30) however, pairwise comparisons indicated weak evidence that the 8ka BP measurements had a smaller spread than the other time periods. To be conservative, we therefore estimated the pooled sample variance amongst *p*-CA levels (around their respective period means) from all samples excluding those in the 8ka period. We then set $\tau_j^2 = \tau$.

Independent estimates of the relative increase in *p*-CA levels from those samples arising during the *Laschamps Event* (covering 600 years in total) against the *p*-CA values from those samples occurring in the other periods were then made using Fieller's test with equal variances (*65*).

Grain Malformation Analysis

Grain Malformation as a Measure of Environmental Stress

The pollen production process (microsporogenesis) is extremely sensitive to environmental stress (*46*). Increased stress exerted on a plant during pollen production can manifest in higher frequencies of pollen malformations. Due to their resistance to decay, these malformed pollen grains are preserved within the paleorecord alongside their phenotypical counterparts. Counting the frequencies of pollen malformations recovered within any records thus provides a paleoenvironmental stress proxy (*42*). Intervals of increased pollen malformations are found during several key extinction events including the end-Permian (*41*, *45*, *66*), the end-Triassic (*43*, *67*, *68*), and the end-Devonian (*5*).

The range of environmental stresses that may lead to increases in pollen malformation is broad, including rapid changes in climate, moisture, and temperature; photochemical and geochemical pollution; and fungal attack/disease. Consequently, one must be careful in ascribing any increase in malformation rate to a specific cause. However, one further factor known to significantly increase malformation rates, and reproduced in controlled laboratory experiments, are heightened levels of UV-B irradiating the plant during pollen production (*1*, *42*).

Grain Malformation Analysis

The quantification of grain malformations was performed concurrently to the py-GC-MS preparations. For each 150yr interval, having obtained concentrated pollen residue from the Suigetsu sediment, a random sample of *Pinus D.* pollen grains were extracted onto a slide. The

total number of *Pinus D.* grains were counted, N_{total}, as well as the number of malformed grains $N_{malformed}$. Phenotypically normal *Pinus D.* pollen grains consist of a central corpus and two sacci (air sacs) attached to the external corpus wall. We considered malformations that consist of grains having fewer than two sacci (panel A in Fig. S5), grains with more than two sacci (panel B), and conjoined or fused grains (panel C) [4]. For our statistical analysis, a specific grain was assessed as malformed if it had any of these three features.

All malformed grains were then removed before isolating the number of grains required for py-GC-MS. This ensured we did not bias the pollen chemistry analysis – the outer walls (exines) of pollen grains are composed of sporopollenin and are more heavily concentrated in the sacci, so we wished to control for the number of sacci in the py-GC-MS analysis.

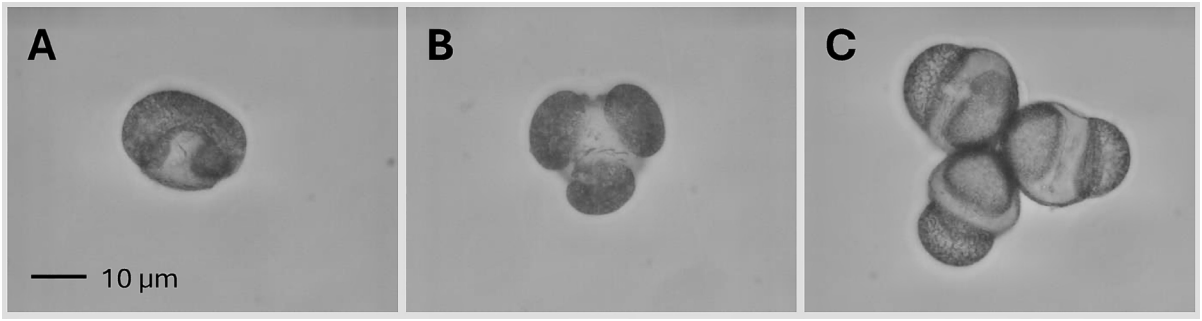

Fig. S5 Types of Pinus D. grain malformations found in the Lake Suigetsu sediment record. Panel A: Grain with single saccus. Panel B: Grain with more than two sacci. Panel C: Conjoined grain.

Logistic Regression on Grain Malformation Counts during the Laschamps Event

We considered a binary logistic regression to model the probability of *Pinus D.* grain malformation p_i in each broad time period. The i^{th} sample, consisting of n_i grains and arising from calendar age θ_i, provided a count of M_i malformations and $n_i - M_i$ phenotypically normal grains. To account for the overdispersion observed across these samples (i.e., the extra variation beyond that attributable to binomial sampling) we used the approach presented by Williams (*48*). We consider μ_i,:

$$\log\frac{\mu_i}{1-\mu_i} = \beta_0 + \beta_1 1[\theta_i = 1.3ka] + \beta_2 1[\theta_i = 8ka] + \beta_3 1[\theta_i = 53ka] + \beta_4 1[\theta_i = 65ka],$$

and introduce independent unobserved variables P_i with $\mathbb{E}[P_i] = \mu_i$, $Var[P_i] = \phi\mu_i(1-\mu_i)$ and assume, conditional on $P_i = p_i$, $M_i \sim Bin(n_i, p_i)$. Here, we use the *Laschamps Event* as our baseline time period to simplify comparison. A summary of the results can be found in Table S2.

Grouping Model	Regression Coefficient			
Explanatory Variable	Estimate	S.E.	95% CI	p-value
Baseline - 41ka Time Period	-4.17	0.26	[-4.67, -3.66]	$< 1 \times 10^{-4}$
1.3ka Time Period	-0.73	0.47	[-1.65, 0.19]	0.12
8ka Time Period	-0.41	0.45	[-1.28, 0.47]	0.37
53ka Time Period	-1.14	0.54	[-2.19, -0.08]	0.04
65ka Time Period	-0.89	0.63	[-2.13, 0.35]	0.16

	Overdispersion Parameter	0.0062	

Table S2 Summary of extra-binomial logistic regression model, where the log-odds of grain malformation are dependent upon overall time period grouping (i.e., 1.3, 8, 41, 53, or 65ka).

Greenhouse Experiment to Understand Effect of UV-B on *p*-CA levels

Notation

When considering UV-B doses, we use the biologically effective ($_{BE}$) radiation as calculated according to Flint's biological spectral weighting function (*49*).

Experimental Design

60 cultivars of *Pinus mugo* var. Mumpitz were sourced from Jens Meyer Jungpflanzen, Germany. Despite their small size (e.g., less than 20 cm in height above ground) they are reproductively fertile, and therefore ideal for experiments under greenhouse conditions. The cultivars were stored in 2L plastic pots, with bark added on the soil surface to protect the soil in the cultivars. The height of the cultivars was approximately 14 cm.

The greenhouse experiment took place at the Arboretum at Milde, University of Bergen, Norway. The greenhouse dimensions are 5 x 3.5 m (length x width) and a maximum of 2.8 m height. Windows are made from a polyester material which blocks UV radiation. In total six individual frames were placed within the greenhouse, with each frame having an experimental area of 83 x 116 cm. Two Q-LAB 313 UV-B fluorescent tubes were placed either side, 10.5 cm from the centre point in each frame. Half of the UV-B fluorescent tubes were wrapped in 0.095 mm cellulose diacetate film (Kotelo-Rauma, Finland) to create a UV-B treatment in each frame. Cellulose diacetate transmits UV-B and UV-A radiation but absorbs the UV-C radiation emitted from the fluorescent tubes. For the control in each frame, the other half of the fluorescent tubes were wrapped in a polyester filter (Autostat CT5, 0.125 x 610 x 1220 mm, MacDermid autotype Ltd) which transmits UV-A but absorbs UV-B and UV-C. The filters were cut to fit around the tubes and held in place by a UV resistant tape.

A polyester film separator was used to divide each frame into two sections, and Rosco 226 UV filter curtains were made to fit the frames so that no UV light was transmitted between frames. UV-B fluorescent lamps were suspended 57 cm above the ground. These lamps were 30 cm above the top of the plants and 44cm from the bottom (as determined by the top of the plant pots). The UV-B lamps were turned on between 11:00 and 17:00 each day, giving an overall UV-B dose of ~21 kJ m^{-2} $day^{-1}{}_{BE}$ at the top of the plants (at 30 cm distance from the lamps) and ~15 kJ m^{-2} $day^{-1}{}_{BE}$ at the bottom of the plants (at 44cm distance). The pollen-producing parts of the UV-B exposed cultivars that we sampled experienced a mean dose of 16.8 kJ m^{-2} $day^{-1}{}_{BE}$ (as estimated at the middle of the plant at 37cm distance from the lamps). There was an Azira 71 air conditioning unit placed in the greenhouse, with a target temperature set to 18ºC. The unit was programmed to turn on if the air temperature in the greenhouse was greater than this target temperature.

Plants were placed into the greenhouse on 19.03.2024 and left for 7 days to acclimatize. When placed in the greenhouse, no visible swelling in buds had occurred. The UV-B dose began on 26.03.2024, and plants were watered regularly (every three days). The location of the plants was randomly shuffled when watered (every third day). Plants were monitored for pollen development daily and sampled in the first instance that inflorescences were producing pollen. Sampling involved placing a paper bag around the inflorescence and then shaking the branch into the bag.

In some instances, the pollen inflorescences were sampled twice (23 instances) or three times (5 instances) as pollen production continued. All samples were kept separate and so, for consistency, we chose to use the first sampling date for analysis in GC-MS in all further analyses. In total 35 trees produced pollen for which a viable sample could be collected using py-GC-MS.

After collection in the greenhouse, the paper bags containing pollen were brought to a laboratory at the Department of Biology, University of Bergen and left to dry at room temperature for 2 days. They were then placed into the freezer at -22°C before further processing. Before preparation for py-GC-MS, the samples were sieved using a 125 µm sieve before being stored in 2 ml Eppendorf tubes.

Subsampling for GC-MS consisted of taking one spatula tip from the original sample, placing it in a new Eppendorf tube and rinsing with ethanol and then water to encourage pollen grains to sink when centrifuged. For each sample replicate, 150 pollen grains were isolated with a drawn-out Pasteur pipette before being transferred to microvials (GL Sciences). The samples were then dried in an oven (50°C) overnight and then placed in the freezer until py-GC-MS analysis. We prepared three replicates per pollen sample.

One tree (ID PU52) produced a large quantity of pollen but was noted to contain underdeveloped sacci and be very pale in comparison to other samples during sample preparation. This tree was therefore excluded from further analyses. py-GC-MS analyses of all the greenhouse pollen samples followed the same procedure as the fossil pollen samples in terms of calibration methodology, replicates and instrumental settings.

A total of 16 cultivars had measurable pollen from the UV-B treatment and 18 cultivars from the control, see Table S3.

Frame	Number of individuals producing pollen	
	Control	UV-B
A	1	3
B	3	2
C	4	2
D	3	5
E	3	1
F	4	3
Total	**18**	**16**

Table S3 Number of cultivars generating pollen in UV-B greenhouse experiment

Analysis and Results

The mean *p*-CA levels (over the three 150 grain replicates) for the first pollen sampling of each of the 18 control cultivars and the 16 cultivars experiencing UV-B treatments are shown in Fig. S6. To enable comparison with the findings from our subfossil pollen groupings (in particular, the relative increase of 31% in *p*-CA recorded during the *Laschamps Event* compared to 1.3 ka BP) we perform an analogous statistical analysis: estimating the relative increase in the amount of *p*-CA in the UV-B exposed cultivars compared to the controls.

Bartlett's test provides no evidence against homogeneity of variance in the recorded mean *p*-CA values between the control and UV-B treatment groups (K^2 statistic = 0.001, df = 1, *p-value* = 0.97). Assuming equal variances for the two groups, application of Fieller's test then provides an estimate that pollen grains from *Pinus mugo* cultivars experiencing the UV-B treatment with an average flux of 16.8 kJ m^{-2} day^{-1}_{BE} have a mean level of *p*-CA that is 1.01 (95% CI of [0.95, 1.07]) times the mean level of those grains in the control group exposed to 0 kJ m^{-2} day^{-1}_{BE}.

Importantly, we can compare this greenhouse-based estimate of the relative increase in in *p*-CA (with a mean UV-B flux of 16.8 kJ m^{-2} day^{-1}_{BE}) with the multiplicative increase in *p*-CA of 1.31 (95% CI [1.19-1.44] recorded when comparing subfossil pollen from the *Laschamps Event* to subfossil pollen at 1.3ka BP. The 95% CI for the relative increase in the greenhouse (from 0 to 16.8 kJ m^{-2} day^{-1}_{BE}) and the 95% CI for the relative increase in our sediment core pollen samples (from 1.3ka BP to 41 ka BP) are disjoint and do not overlap. Furthermore, the UV-B flux at 1.3ka BP will have been greater than the greenhouse control of 0 kJ m^{-2} day^{-1}_{BE} and so pollen from this 1.3ka BP period would be expected to have a higher mean p-CA level than the greenhouse no-UV-B controls. Consequently, assuming that *Pinus mugo* is a valid analogue for our *Pinus D.* subfossil pollen, we estimate that during the 600yr interval we sample over the *Laschamps Event*, the mean UV-B flux was significantly greater than 16.8 kJ m^{-2} day^{-1}_{BE} (the mean UV-B dose to which the greenhouse-based cultivars were exposed).

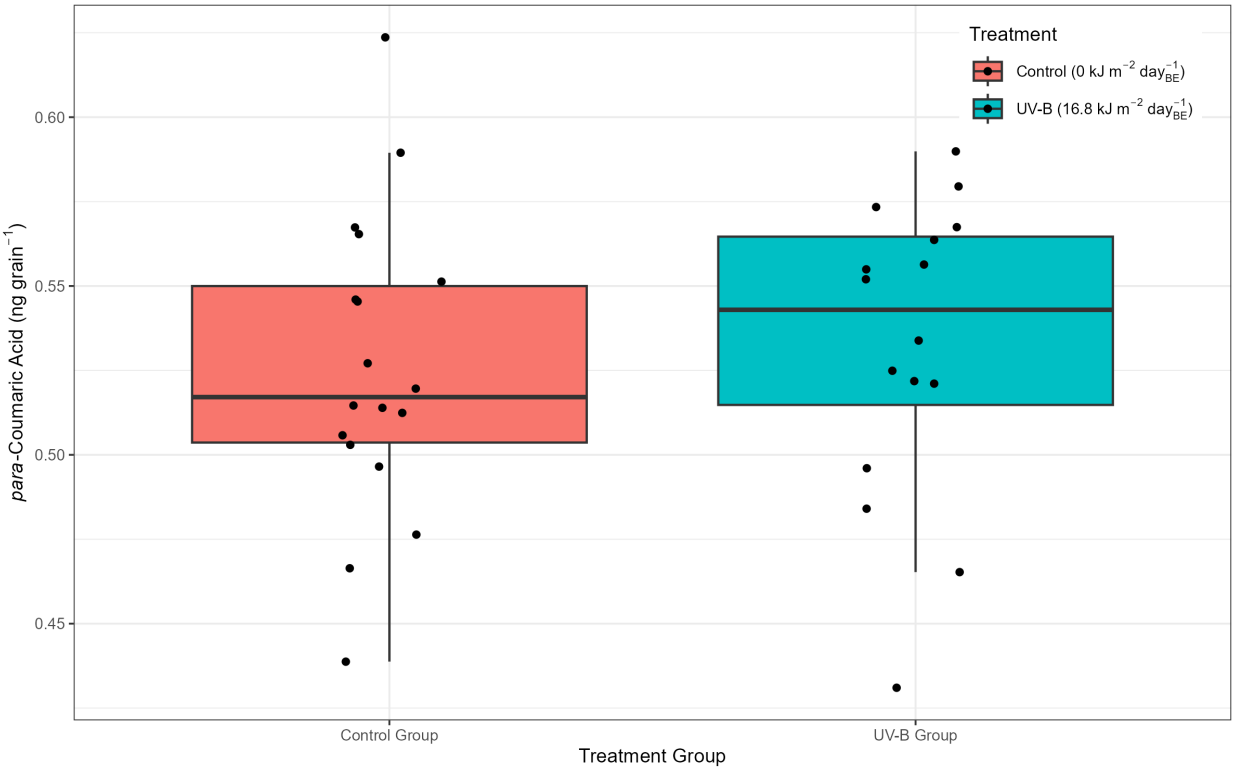

Fig. S6 Levels of p-CA in Pinus mugo cultivars exposed to UV-B radiation compared to control cultivars in greenhouse experiment. Boxplots of mean p-CA levels (over three replicates) per pollen grain in 18 control cultivars (exposed to UV-B flux of 0 kJ m^{-2} day^{-1}_{BE}) and 16 UV-B exposed cultivars (exposed to a mean UV-B flux of 16.8 kJ m^{-2} day^{-1}_{BE}). Solid dots show the mean p-CA level recorded in each individual cultivar.

Comparison with Modern Day UV-B Flux and Relative Increase during the Laschamps Event

We wish to compare our estimated lower bound of 16.8 kJ m^{-2} day^{-1}_{BE} on the mean UV-B flux during the *Laschamps Event* with present-day UV-B irradiances, to understand the relative increase. Information on UV-B fluxes from Lake Suigetsu (35˚ 35' N, 0m amsl) itself is not available, so we instead use daily measurements from Raleigh, N. Carolina US that is available from the USDA at https://uvb.nrel.colostate.edu/UVB/. Raleigh should provide a close analogue to Suigetsu being at an almost identical latitude (35˚ 73' N) and altitude (120m amsl). To calculate the analogous present-day UV-B fluxes, we use the average of the daily measurements from 1st March - 31st May (the expected period of pollen production for *Pinus D.*) in each year from 2005–2024 (although we note that the years 2020 and 2021 are entirely missing from the USDA database due to the impact of COVID-19). This provides an estimate of the present-day mean UV-B flux of 14.3 kJ m^{-2} day^{-1}_{BE}. Our lower bound estimate of 16.8 kJ m^{-2} day^{-1}_{BE} for the flux during the period sampled from 41.3-40.7ka BP would therefore correspond to a lower bound of 18% for the mean increase in the surface UV-B flux compared to present day that extends over the full 600yr period sampled during the *Laschamps Event*. This lower bound of 18% for the relative increase in surface UV-B flux over the period from 41.3-40.7ka BP compared to present day is greater than the model-based 10–15% increase estimated for the concurrence of the *Laschamps Event* with a Grand Solar Minimum (*9*); but below the 20-30% increase modelled by a coincident extreme solar particle event (*8*).